Theory and Experiment of Novel Microstrip Slow-Wave Open-Loop Resonator Filters

Jia-Sheng Hong, *Member, IEEE,* and Michael J. Lancaster, *Member, IEEE*

***Abstract*— This paper presents the theory and experiment of a new class of microstrip slow-wave open-loop resonator filters. A comprehensive treatment of capacitively loaded transmission line resonator is described, which leads to the invention of microstrip slow-wave open-loop resonator. The utilization of microstrip slow-wave open-loop resonators allows various filter configurations including those of elliptic or quasi-elliptic function response to be realized. The filters are not only compact size due to the slow-wave effect, but also have a wider upper stopband resulting from the dispersion effect. These attractive features make the microstrip slow-wave open-loop resonator filters hold promise for mobile communications, superconducting and other applications. Two filter designs of this type are described in detail. The experimental results are demonstrated and discussed.**

***Index Terms*— Microstrip filters, slow-wave open-loop resonators.**

I. Introduction

IN MANY APPLICATIONS, keeping filter structures to a minimum size and weight is very important. It would seem that planar filter structures which can be fabricated using printed-circuit technologies would be preferred whenever they are available and are suitable because of smaller sizes and lighter weight. Recent advance in high-temperature superconducting (HTS) circuits and microwave monolithic integrated circuits (MMIC) has additionally stimulated the development of various planar filters, especially narrow-band bandpass filters which play an important role in modern communications systems [1], [2]. In order to reduce interference by keeping out-of-band signals from reaching a sensitive receiver, a wider upper stopband, including $2f_0$, where f_0 is the midband frequency of a bandpass filter, may also be required. However, many planar bandpass filters which are comprised of half-wavelength resonators have inherently a spurious passband at $2f_0$. A cascaded low-pass filter or bandstop filter may be used to suppress the spurious passband at the cost of extra insertion loss and size. Although quarter-wavelength resonator filters have the first spurious passband at $3f_0$, they require short-circuit (grounding) connections with via holes, which is not quite compatible with planar fabrication techniques. Lumped element filters ideally do not have any spurious passband at all, but they suffer from higher loss and poorer power handling capability. Bandpass filters using stepped impedance resonators (SIR) [3] or end-coupled slow-wave resonators [4] are able to control spurious response, but they can only be implemented in few filtering configurations.

In this paper, we introduce a new class of microstrip bandpass filters based on coupled slow-wave open-loop resonators. We show that the use of slow-wave open-loop resonators enable various filters including those of elliptic or quasi-elliptic function response to be designed, that are not only compact size, but that also have a wide upper stopband. In Section II, we present a comprehensive circuit theory of capacitively loaded transmission line resonator. This is necessary because it leads to the invention of microstrip slow-wave open-loop resonator which is described in Section III, where the full-wave electromagnetic (EM) simulation confirms the circuit theory. The designs of a five-pole direct-coupling filter and a four-pole cross-coupled filter using microstrip slow-wave open-loop resonators are described in detail in Sections IV and V, respectively, including the characterization of coupling coefficients. The experimental results of the filters are also demonstrated and discussed. Conclusions are followed in Section VI.

II. Capacitively Loaded Transmission Line Resonator

For our purpose, let us consider at first a capacitively loaded lossless transmission line resonator of Fig. 1(a), where $C_{\rm L}$ is the loaded capacitance; Z_a, β_a, and d are the characteristic impedance, the propagation constant, and the length of the unloaded line, respectively. Thus, the electric length $\theta_a = \beta_a d$. The circuit response of Fig. 1(a) may be described by

$$\begin{bmatrix} V_1 \\ I_1 \end{bmatrix} = \begin{bmatrix} A & B \\ C & D \end{bmatrix} \cdot \begin{bmatrix} V_2 \\ -I_2 \end{bmatrix} \tag{1}$$

with

$$A = D = \cos\theta_a - \tfrac{1}{2}\omega C_{\rm L} Z_a \sin\theta_a \tag{2a}$$

$$B = jZ_a \sin\theta_a \tag{2b}$$

$$C = j\left(\omega C_{\rm L}\cos\theta_a + \frac{1}{Z_a}\sin\theta_a - \frac{1}{4}\omega^2 C_{\rm L}^2 Z_a \sin\theta_a\right) \tag{2c}$$

where $\omega = 2\pi f$ is the angular frequency; A, B, C, and D are the network parameters of transmission matrix, which also satisfy the reciprocal condition $AD - BC = 1$.

Assume that a standing wave has been excited subject to the boundary conditions $I_1 = I_2 = 0$. For no vanished V_1 and V_2, it is required that

$$\frac{C}{A} = \left.\frac{I_1}{V_1}\right|_{I_2=0} = \left.\frac{I_2}{V_2}\right|_{I_1=0} = 0. \tag{3}$$

Manuscript received March 17, 1997; revised August 18, 1997.

The authors are with the School of Electronic and Electrical Engineering, University of Birmingham, Edgbaston, Birmingham B15 2TT, U.K.

Publisher Item Identifier S 0018-9480(97)08355-5.

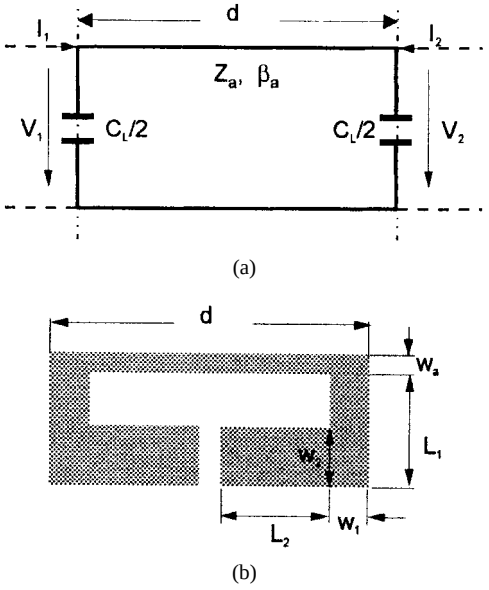

Fig. 1. (a) Capacitively loaded transmission line resonator and (b) a microstrip slow-wave open-loop resonator on substrate (not shown).

Because

$$A = \left.\frac{V_1}{V_2}\right|_{I_2=0} = \begin{cases} -1, & \text{for the fundamental resonance} \\ 1, & \text{for the first spurious resonance} \end{cases} \tag{4}$$

we have from (2a) that

$$\cos\theta_{a0} - \tfrac{1}{2}\omega_0 C_{\mathrm{L}} Z_a \sin\theta_{a0} = -1 \tag{5a}$$

$$\cos\theta_{a1} - \tfrac{1}{2}\omega_1 C_{\mathrm{L}} Z_a \sin\theta_{a1} = 1 \tag{5b}$$

where the subscripts 0 and 1 indicate the parameters associated with the fundamental and the first spurious resonance, respectively. Substituting (5a) and (5b) into (2c), and letting $C = 0$ according to (3), yield

$$\frac{\omega_0 C_{\mathrm{L}}}{2}(1 - \cos\theta_{a0}) = \frac{1}{Z_a}\sin\theta_{a0} \tag{6a}$$

$$\frac{\omega_1 C_{\mathrm{L}}}{2}(1 + \cos\theta_{a1}) = -\frac{1}{Z_a}\sin\theta_{a1}. \tag{6b}$$

These two eigenequations can further be expressed as

$$\theta_{a0} = 2\tan^{-1}\left(\frac{1}{\pi f_0 Z_a C_{\mathrm{L}}}\right) \tag{7a}$$

$$\theta_{a1} = 2\pi - 2\tan^{-1}(\pi f_1 Z_a C_{\mathrm{L}}) \tag{7b}$$

from which the fundamental resonant frequency f_0 and the first spurious resonant frequency f_1 can be determined. Now it can clearly be seen from (7a) and (7b) that $\theta_{a0} = \pi$ and $\theta_{a1} = 2\pi$ when $C_{\mathrm{L}} = 0$. This is the case for the unloaded half-wavelength resonator. For $C_{\mathrm{L}} \neq 0$, it can be shown that the resonant frequencies are shifted down as the loading capacitance is increased, indicating the slow-wave effect. For the demonstration Fig. 2 plots the calculated resonant frequencies according to (7a) and (7b), as well as their ratio for different capacitance loading when $Z_a = 52\ \Omega$, $d = 16$ mm and the associated phase velocity $v_{pa} = 1.1162 \times 10^8$ m/s. As can be seen when the loading capacitance is increased, in addition to the decrease of both resonant

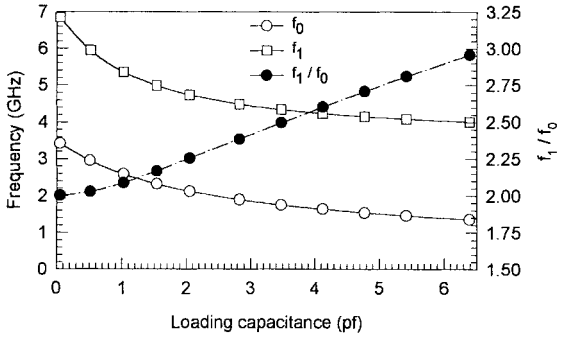

Fig. 2. Calculated fundamental and first spurious resonant frequencies of a capacitively loaded transmission line resonator, as well as their ratio against loading capacitance, obtained using a circuit mode.

frequencies, however, the ratio of the first spurious resonant frequency to the fundamental one is increased. To understand the physical mechanism that underlines this phenomenon, which is important for our applications, we may consider the circuit of Fig. 1(a) as a unit cell of a periodically loaded transmission line. This is plausible as we may mathematically expand a function defined in a bounded region into a periodic function. Let β be the propagation constant of the capacitively loaded lossless periodic transmission line. Applying Floquet's theorem [5], i.e.,

$$\begin{aligned} V_2 &= e^{-j\beta d} V_1 \\ -I_2 &= e^{-j\beta d} I_1 \end{aligned} \tag{8}$$

to (1) results in

$$\begin{bmatrix} A - e^{j\beta d} & B \\ C & D - e^{j\beta d} \end{bmatrix} \cdot \begin{bmatrix} V_2 \\ -I_2 \end{bmatrix} = \begin{bmatrix} 0 \\ 0 \end{bmatrix}. \tag{9}$$

A nontrivial solution for V_2, I_2 exists only if the determinant vanishes. Hence,

$$(A - e^{j\beta d})(D - e^{j\beta d}) - BC = 0. \tag{10}$$

Since $A = D$ for the symmetry and $AD - BC = 1$ for the reciprocity, the dispersion equation of (10) becomes

$$\cos(\beta d) = \cos\theta_a - \tfrac{1}{2}\omega C_{\mathrm{L}} Z_a \sin\theta_a \tag{11}$$

according to (2a)–(2c).

Because the dispersion equation governs the wave propagation characteristics of the loaded line, we can substitute (7a) and (7b) into (11) for those particular frequencies. It turns out that $\cos(\beta_0 d) = -1$ for the fundamental resonant frequency and $\cos(\beta_1 d) = 1$ for the first spurious resonant frequency. As $\beta_0 = \omega_0/v_{p0}$ and $\beta_1 = \omega_1/v_{p1}$, where v_{p0} and v_{p1} are the phase velocities of the loaded line at the fundamental and the first spurious resonant frequencies, respectively, we obtain

$$\frac{f_1}{f_0} = 2\frac{v_{p1}}{v_{p0}}. \tag{12}$$

If there were no dispersion the phase velocity would be a constant. This is only true for the unloaded line. However, for the periodically loaded line the phase velocity is frequency dependant. It would seem that, in our case , the increase in ratio of the first spurious resonant frequency to the fundamental one when the capacitive loading is increased would attribute to the increase of the dispersion. This may clearer be seen from the dispersion curves plotted in Fig. 3, which are obtained

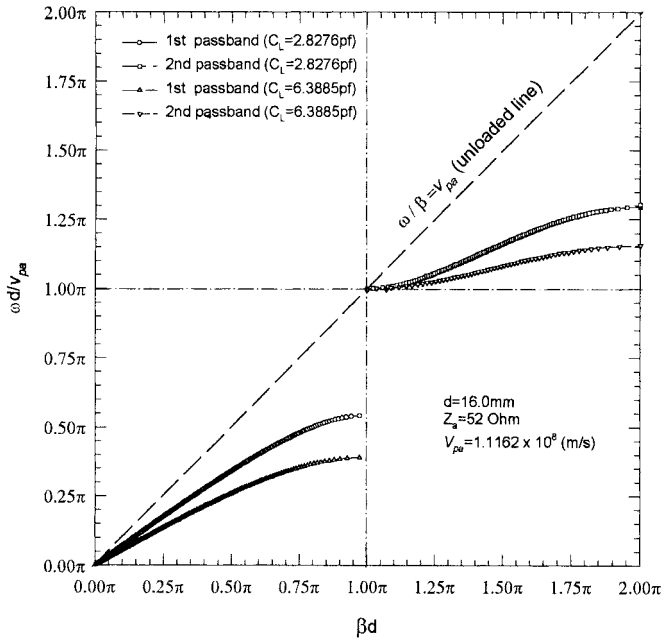

Fig. 3. Dispersion curves of a capacitively loaded lossless transmission line.

from (11). Notice that the vertical axis is normalized with respect to v_{pa}, the phase velocity of the unloaded line. Thus, the normalized phase velocity for any point on the dispersion curves is given by the slope of the line joining the point to the origin. The diagonal broken line has a constant slope of 1, representing the nondispersion characteristic of the unloaded line ($C_{\rm L} = 0$). However, for any $C_{\rm L} > 0$ the slope dose not keep constant anymore, indicating the dispersion. As the loading capacitance $C_{\rm L}$ is increased, the slope or the phase velocity is decreased, which is also applicable for both the fundamental and the first spurious resonance occurring at $\beta d = \beta_0 d = \pi$ and $\beta d = \beta_1 d = 2\pi$, respectively. This is what would be expected for the slow-wave effect. On the other hand, one can also easily find from Fig. 3 that for a given $C_{\rm L}$, the slope or the phase velocity of the first spurious resonance is larger than that of the fundamental resonance, and the difference between these two increases when $C_{\rm L}$ is increased. This, together with (12), would confirm that the dispersion effect indeed accounts for the increase in ratio of the first spurious resonant frequency to the fundamental one. Therefore, this property can be used to design the bandpass filter with a wider upper stopband.

III. Slow-Wave Open-Loop Resonator

It is obvious that based on the circuit model of Fig. 1(a) different resonator configurations may be realized. Herein, we propose a so-called microstrip slow-wave open-loop resonator, which is composed of a microstrip line with both ends loaded with folded open-stubs as Fig. 1(b) shows. The folded arms of open-stubs are not only for increasing the loading capacitance to ground as referred to Fig. 1(a), but also for the purpose of interstage or cross couplings. Shown in Fig. 4 are the fundamental and first spurious resonant frequencies as well as their ratio against the length of folded open-stub, obtained using a full-wave electromagnetic (EM) simulator [7]. Note

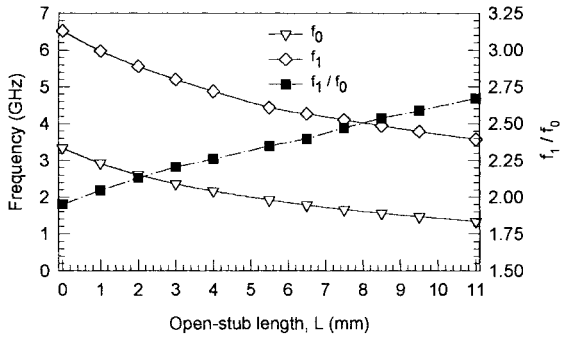

Fig. 4. Simulated fundamental and first spurious resonant frequencies of a microstrip slow-wave open-loop resonator, as well as their ratio against the loading open-stub, obtained using a full-wave EM simulator.

that in this case the length of folded open-stub is defined as $L = L_1$ for $L \leq 5.5$ mm and $L = 5.5 + L_2$ for $L > 5.5$ mm as referring to Fig. 1(b). One can see that the results obtained by the full-wave EM simulation bear the similarity to those obtained by the circuit theory shown in Fig. 2. This is what would be expected because in this case the unloaded microstrip line, which has a length of $d = 16$ mm and a width of $w_a = 1.0$ mm on a substrate with a relative dielectric constant of 10.8 and a thickness of 1.27 mm, exhibits about the same parameters of Z_a and v_{pa} as those assumed in Fig. 2, while the open-stub could approximate to the lumped capacitor. At this stage, it may be worthwhile pointing out that to approximate to the lumped capacitor, it is essential that the open-stub should have a wider line or lower characteristic impedance. In this case, by referring to Fig. 1(b), we have $w_1 = 2.0$ mm and $w_2 = 3.0$ mm for the folded open-stub. It should be mentioned that the slow-wave open-loop resonator differs from the miniaturized hairpin-resonator [6] primarily in that they are developed from rather different concepts and purposes. The latter is developed from conventional hairpin resonator by increasing capacitance between both ends to reduce the size of the conventional hairpin resonator [6]. The main advantage of microstrip slow-wave open-loop resonator of Fig. 1(b) over the previous ones is that various filter structures (see Fig. 5) can be developed, including canonical filter in Fig. 5(d) and cascaded quadruplet (CQ) filter in Fig. 5(e) which exhibit elliptic or quasi-elliptic function response.

IV. Five-Pole Direct Coupling Filter

For our demonstration we will focus on two examples of narrow-band microstrip slow-wave open-loop resonator filters. The first one is a five-pole direct-coupling filter with overlapped coupled slow-wave open-loop resonators as Fig. 5(c) shows. This filter was originally developed to meet the following specifications for an instrumentation application: As

Center frequency	1335 MHz
3-dB bandwidth	30 MHz
Passband loss	3 dB Max
Min stopband rejection	dc to 1253 MHz, 60 dB
	1457–2650 MHz, 60 dB
	2650–3100 MHz, 30 dB
60-dB bandwidth	200 MHz Max

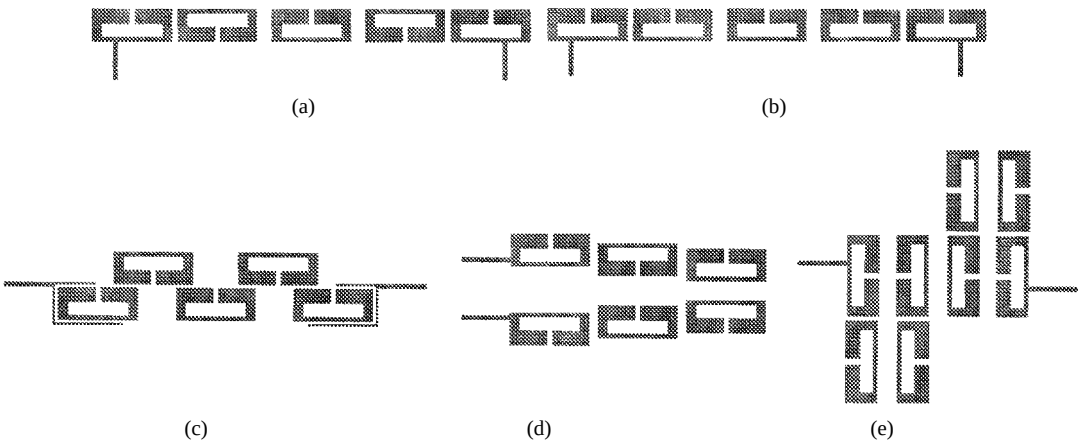

Fig. 5. Some filter structures realized using microstrip slow-wave open-loop resonators: (a), (b), and (c) directive coupling filters; (d) canonical filter; and (e) cascaded quadruplet (CQ) filter.

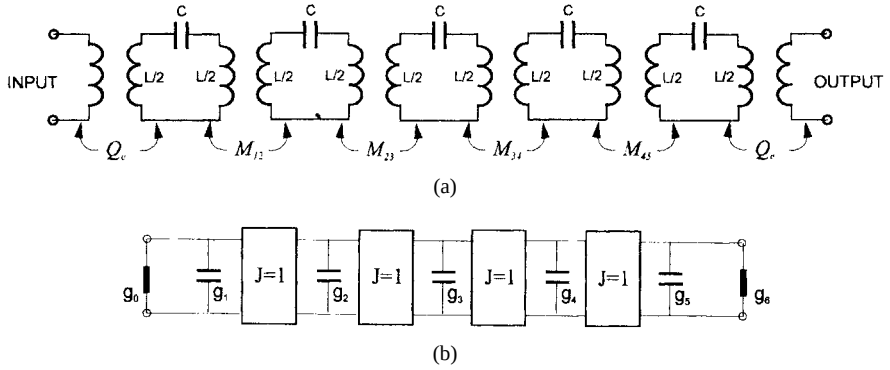

Fig. 6. (a) An equivalent circuit of the five-pole directive coupling bandpass filter and (b) an associated low-pass prototype filter.

can be seen a wide upper stopband including $2f_0$ is required and at least 30-dB rejection at $2f_0$ is needed.

The bandpass filter may be represented by an equivalent circuit shown in Fig. 6(a), where $1/\sqrt{LC} = \omega_0$ is the center angular frequency of the filter; M_{12}, M_{23}, $\cdots$, M_{45} are the coupling coefficients between adjacent resonators, and Q_e is the external quality factor denoting the input and output coupling. The coupling coefficients and external quality factor may be synthesized from a low-pass prototype filter shown in Fig. 6(b), where the rectangular boxes represent frequency invariant immittance inverters defined through a transmission matrix of the form [8]

$$\begin{bmatrix} 0 & j/J \\ jJ & 0 \end{bmatrix} \tag{13}$$

in which J is the characteristic admittance of the inverter, and in our case $J = 1$. The other elements g_1, g_2, $\cdots$, g_5 of the prototype filter could be determined by synthesizing a standard Chebyshev filter. The external quality factor and coupling coefficients can then be found by

$$\begin{aligned} Q_e &= \frac{g_0 g_1}{\text{FBW}} \\ M_{12} &= M_{45} = \frac{\text{FBW}}{\sqrt{g_1 g_2}} \\ M_{23} &= M_{34} = \frac{\text{FBW}}{\sqrt{g_2 g_3}} \end{aligned} \tag{14}$$

where FBW denotes the fractional bandwidth of bandpass filter. Considering the effect of conductor loss that is the narrower the bandwidth, the higher is the insertion loss, which is even higher at the passband edges because the group delay is usually longer at the passband edges, we designed the filter with a slightly wider FBW, trying to meet the 3-dB bandwidth of 30 MHz as specified, and found

$$\begin{aligned} M_{12} &= M_{45} = 0.0339 \\ M_{23} &= M_{34} = 0.0235 \\ Q_e &= 22.4382\,. \end{aligned} \tag{15}$$

The next step of the filter design was to characterize the couplings between adjacent microstrip slow-wave open-loop resonators as well as the external quality factor of the input or output microstrip slow-wave open-loop resonator. The coupling M_{ij} of any pair of adjacent resonators may be characterized by [9]

$$M_{ij} = \frac{f_{p2}^2 - f_{p1}^2}{f_{p2}^2 + f_{p1}^2} \tag{16}$$

where f_{p1} and f_{p2} are the lower and higher split resonant frequencies of a pair of coupled resonators when they are decoupled from the remainder. The external quality factor may be characterized by

$$Q_e = \frac{f_0}{\delta f_{3\,\text{dB}}} \tag{17}$$

where f_0 and $\delta f_{3\,\text{dB}}$ are the resonant frequency and the 3-dB bandwidth of the input or output resonator when it alone is externally excited. Because the split resonant frequencies of coupled resonators and the 3-dB bandwidth of the input

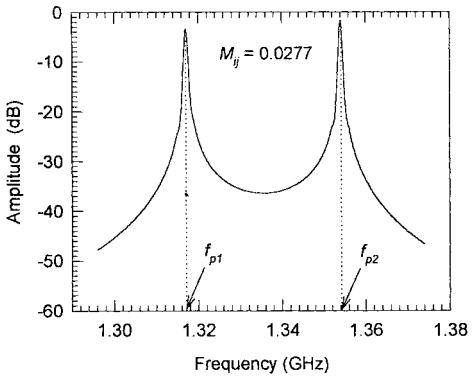

(a)

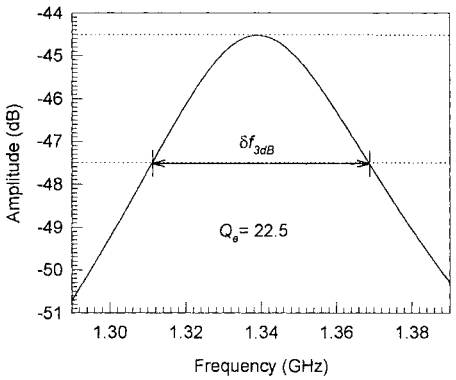

(b)

Fig. 7. (a) Typical frequency responses simulated for extracting the coupling coefficient. (b) Typical frequency responses simulated for extracting the external quality factor.

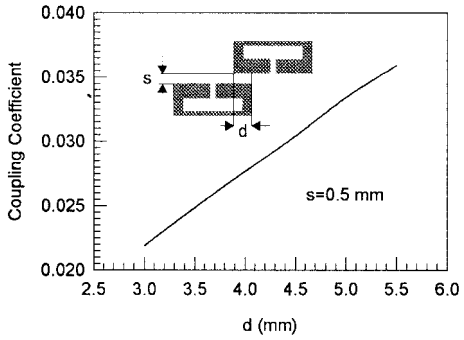

(a)

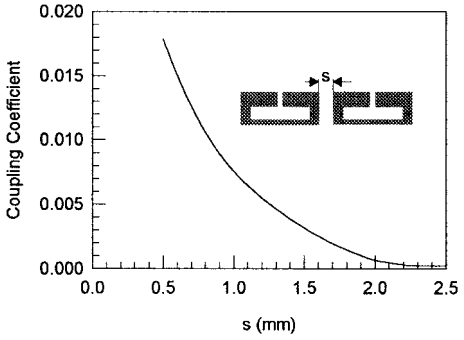

(b)

Fig. 8. Modeled coupling coefficients of (a) overlapped coupled and (b) end-coupled slow-wave open-loop resonators.

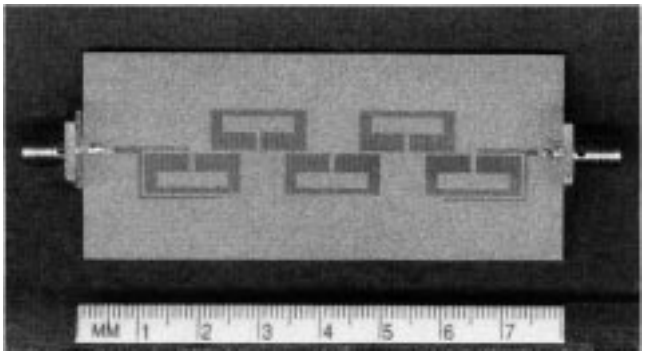

Fig. 9. A photograph of the fabricated five-pole bandpass filter using microstrip slow-wave open-loop resonators.

or output resonator are quite easily identified in full-wave EM simulation, we used the full-wave EM simulator [7] to model the coupling coefficients and external Q. Shown in Fig. 7(a) and (b) are the typical frequency responses obtained from the EM simulation for extracting coupling coefficient and external Q, respectively. Fig. 8(a) depicts the extracted coupling coefficient against different overlapped length d for a fixed coupling gap s, where the size of the resonator is 16 mm by 6.5 mm on a substrate with a relative dielectric constant of 10.8 and a thickness of 1.27 mm. One can see that the coupling almost increases linearly with the overlapped length. It can also be shown that for a fixed d reducing or increasing coupling gap s increases or decreases the coupling. From the filter configuration of Fig. 5(c), one might expect the cross coupling between nonadjacent resonators. We investigated this issue and found that the cross coupling between nonadjacent resonators is quite small when the separation between them is larger than 2 mm as Fig. 8(b) shows. This, however, suggests that the filter configuration of Fig. 5(b) would be more suitable for very narrow-band realization which requires very weak coupling between resonators. Having characterized the couplings we designed the filter with the aid of the EM simulator. The filter was then fabricated on a RT/Duroid substrate. Fig. 9 shows a photograph of the fabricated filter. The size of this five-pole filter is about 0.70 λ_{go} by 0.15 λ_{go}, where λ_{go} is the guided wavelength of a 50-Ω line on the substrate at the midband frequency. Fig. 10 shows experimental results, which represent the first design iteration. Fig. 10(a) gives the details of the passband while Fig. 10(b) shows the wide-band response. Except for a slight deviation in the center frequency and bandwidth, the filter had a midband loss less than 3 dB and exhibited the excellent stopband rejection. It can be seen that more than 50-dB rejection at $2f_o$ has been achieved.

V. Four-Pole Cross-Coupled Filter

The second trial microstrip slow-wave open-loop resonator filter is that of four-pole cross-coupled filter that is a basic unit of CQ [10] filter of Fig. 5(e). It should be noticed that in this case the CQ filter structure is the same as the canonical one of Fig. 5(d). Shown in Fig. 11(a) is an equivalent circuit of the filter, where M_{14} denotes the cross coupling between the input and output resonators. This bandpass filter could be synthesized with the aid of a low-pass prototype filter of

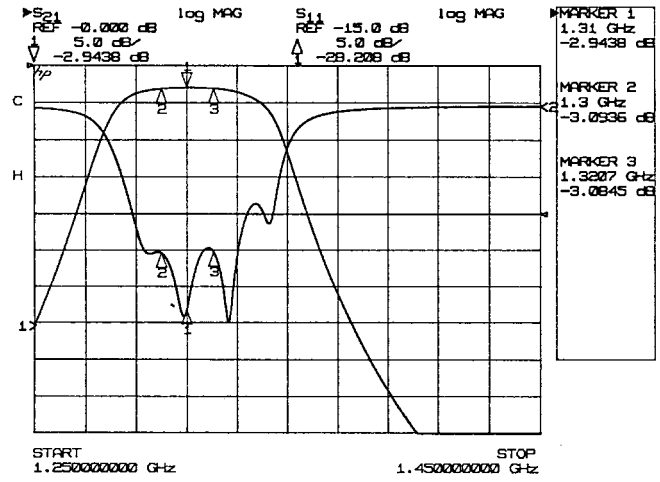

(a)

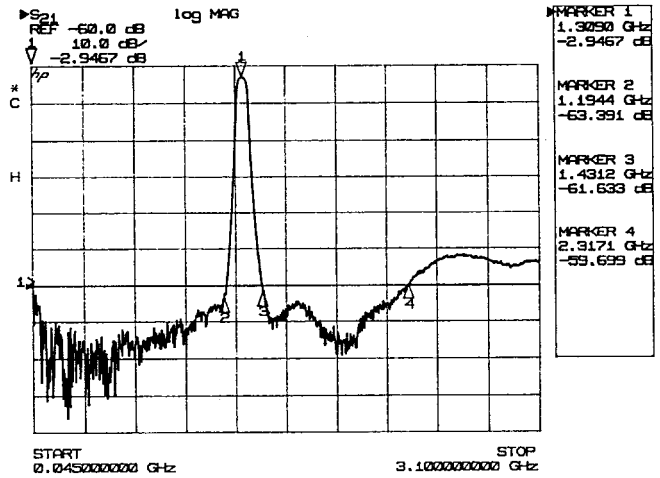

(b)

Fig. 10. Measured filter performance for the five-pole slow-wave open-loop resonator filter. (a) The details of passband response and (b) the wide-band response.

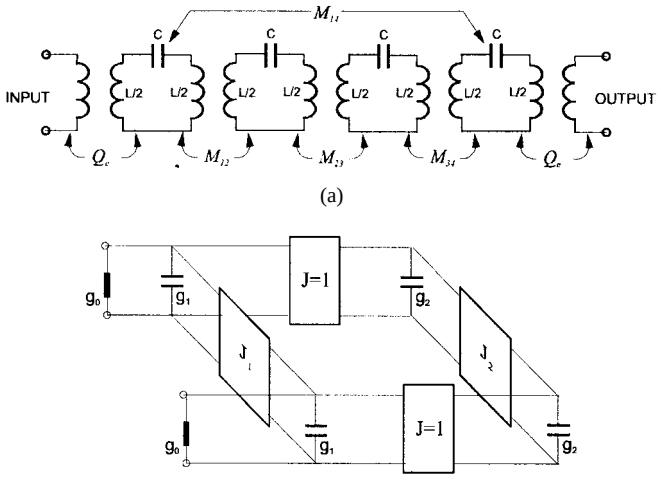

(a)

(b)

Fig. 11. (a) An equivalent circuit of the four-pole cross-coupled bandpass filter and (b) an associated low-pass prototype filter.

Fig. 11(b), whose element values may be obtained using a method described in [11]. Once the element values are found, the external quality factor Q_e and the coupling coefficients of the filter can be calculated by

$$\begin{aligned} Q_e &= \frac{g_0 g_1}{\text{FBW}} \\ M_{12} &= M_{34} = \frac{\text{FBW}}{\sqrt{g_1 g_2}} \\ M_{23} &= \frac{\text{FBW} \cdot J_2}{g_2} \\ M_{14} &= \frac{\text{FBW} \cdot J_1}{g_1}. \end{aligned} \tag{18}$$

The calculated design parameters of the four-pole cross-coupled bandpass filter are listed below

$$\begin{aligned} Q_e &= 26.975 \\ M_{12} &= M_{34} = 0.0297 \\ M_{23} &= 0.0241 \\ M_{14} &= -0.003. \end{aligned} \tag{19}$$

Next, the coupling coefficients of three basic coupling structures encountered in this filter were modeled using the similar approach as described in the last section. The results are depicted in Fig. 12. Notice that the mixed and magnetic couplings are used to realize $M_{12} = M_{34}$ and M_{23}, respectively. While the electric coupling is used to achieve the cross coupling M_{14}. The tapped line input or output was used in this case and the associated external Q could be characterized by the method mentioned before. The filter was designed and fabricated on a RT/Duroid 6010 substrate with a relative dielectric constant of 10.8 and a thickness of 1.27 mm. Fig. 13 shows a photograph of the fabricated four-pole cross-coupled filter. In this case, the size of the filter amounts only to 0.18 λ_{go} by 0.36 λ_{go}. The measured filter performance is illustrated in Fig. 14. The measured 3 dB bandwidth is about 4% at 1.3 GHz. The minimum passband loss was approximately 2.7 dB. The filter exhibited a wide upper stopband with a rejection better than 40 dB up to about 3.4 GHz. The two transmission zeros that are the typical elliptic function response can also clearly be observed. However, the locations of transmission zeros are asymmetric. It would seem that this is mainly resulted from a frequency-dependent cross coupling.

To investigate this issue, we have simulated the field distributions of resonators 1 and 4 against frequencies using the full-wave EM simulation. It turns out that the charge or the electric field density at the upper rejection frequency is higher than that at the lower rejection frequency. This would mean that the electric coupling is stronger at the upper rejection frequency than that at the lower one. As the cross coupling is resulted from the electric coupling between resonators 1 and 4, the stronger the cross coupling, the closer is the transmission zero approaching to the passband edge. This could account for the asymmetric frequency response of Fig. 14. We have then assumed a frequency-dependent cross coupling in a circuit mode of the filter, and obtained a theoretical prediction in Fig. 15, showing an asymmetric frequency response being consistent with the experimental one. Having found the possible cause for the asymmetry

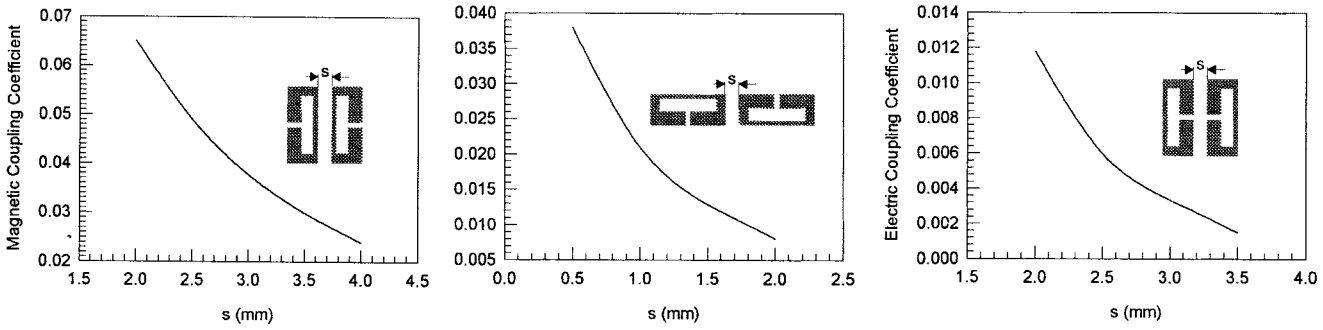

(a) (b) (c)

Fig. 12. Modeled coupling coefficients of coupled microstrip slow-wave open-loop resonators. (a) Magnetic coupling, (b) mixed coupling, and (c) electric coupling.

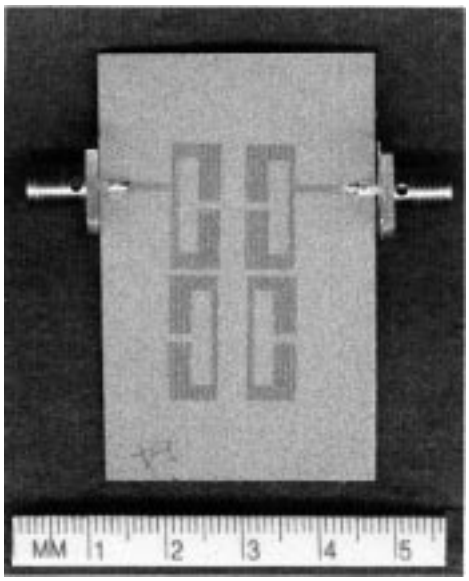

Fig. 13. A photograph of the fabricated four-pole bandpass filter using microstrip slow-wave open-loop resonators.

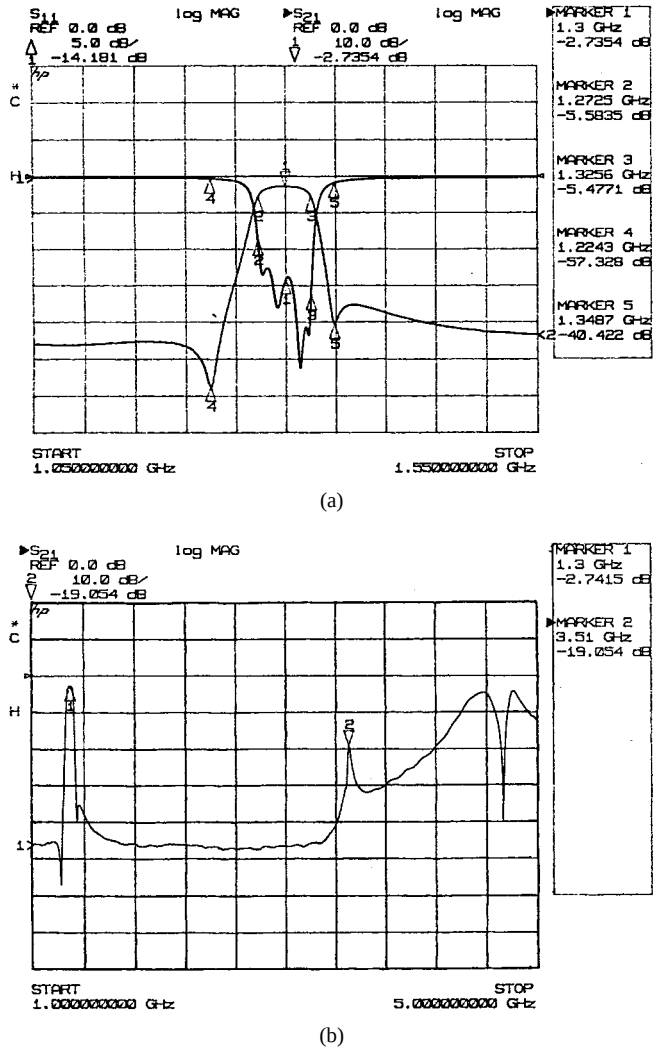

(a) (b)

Fig. 14. Measured filter performance for the four-pole slow-wave open-loop resonator filter exhibiting elliptic function response. (a) The details of pass-band response and (b) the spurious response.

of transmission zeros, we have experimentally attempted to compensate for the frequency-dependent cross coupling. This was done by inserting a tuning element between the coupling gap of resonators 1 and 4. This approach was justifiable on a fact that the charge distributions of coupled resonators are different at the upper and lower rejection frequencies as observed from the full-wave EM simulation. Hence, depending on the tuning element position, the coupling at the upper and lower rejection frequencies could somewhat be balanced. The feasibility of this approach was confirmed by the experiment and the final experimental result is shown in Fig. 16, where a significant improvement in symmetric response is evident.

VI. Conclusion

We have presented both the theory and experiment of a new class of planar microwave bandpass filters using microstrip slow-wave open-loop resonators. The theoretical treatment of capacitively loaded transmission line resonator has not only led to the invention of microstrip slow-wave open-loop resonators, but also given an insight into the properties of this type of resonators. We have performed the full-wave EM simulation to confirm the circuit theory. It has been demonstrated that the use of the microstrip slow-wave open-loop resonators allows various filter configurations including those of elliptic or quasi-elliptic function response to be realized that are not only compact size due to the slow-wave effect, but that also have a wider upper stopband resulted from

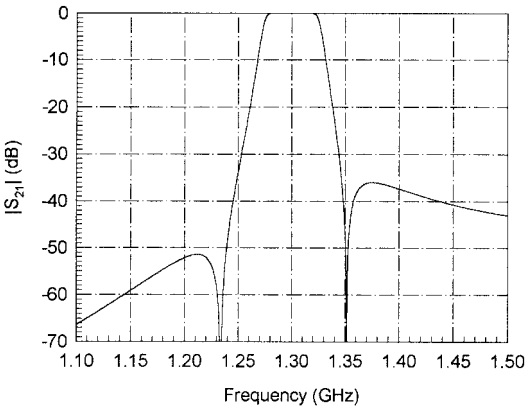

Fig. 15. Theoretical prediction of asymmetric frequency response resulted from a frequency-dependent cross coupling.

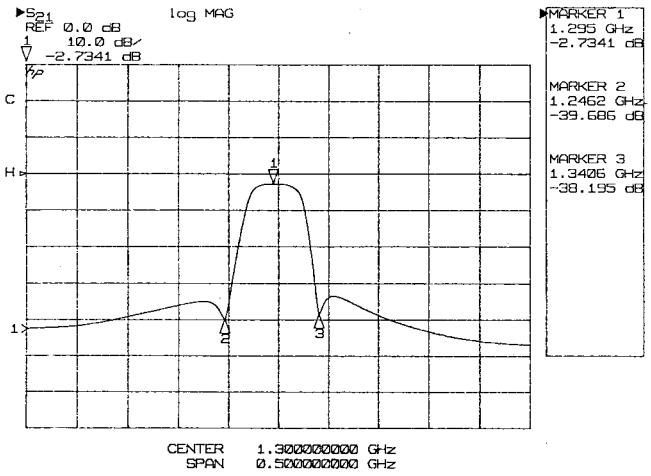

Fig. 16. Measured filter performance of the four-pole slow-wave open-loop resonator filter using the tuning element to compensate for the frequency-dependent cross coupling.

the dispersion effect. We have described in detail the two filter designs using microstrip slow-wave open-loop resonators. It has been shown that the design parameters can be obtained based on the prototype circuits, and the coupling coefficients and external quality factor associated with the microstrip slow-wave open-loop resonators can be characterized in the light of the full-wave simulation. We have discussed the experimental results of the filters and investigated in particular the asymmetric response of cross-coupled filter. It has been found that the asymmetric locations of transmission zeros would attribute to the frequency-dependent cross coupling, and a practical approach using the tuning element has been sought for the compensation. The further experimental result of four-pole cross-coupled filter has verified the feasibility of the approach. It can be seen that the microstrip slow-wave open-loop resonator filters hold promise for mobile communications, HTS, and other applications.

REFERENCES

[1] A. F. Sheta, K. Hettak, J. Ph. Coupez, C. Person, S. Toutain, and J. P. Blot, "A new semi-lumped microwave filter structure," in *1995 IEEE MTT-S Dig.*, pp. 383–386.

[2] G. L. Matthaei, N. O. Fenzi, R. Forse, and S. Rohlfing, "Narrow-band hairpin-comb filters for HTS and other applications," in *1996 IEEE MTT-S Dig.*, pp. 457–460.

[3] M. Makimoto and S. Yamashita, "Bandpass filters using parallel coupled stripline stepped impedance resonators," *IEEE Trans. Microwave Theory Tech.*, vol. MTT-28, pp. 1413–1417, 1980.

[4] J. S. Hong and M. J. Lancaster, "End-coupled microstrip slow-wave resonator filter," *Electron. Lett.*, vol. 32, pp. 1494–1496, 1996.

[5] A. F. Harvey, "Periodic and guided structures at microwave frequencies," *IRE Trans. Microwave Theory Tech.*, vol. MTT-8, pp. 30–61, 1960.

[6] M. Sagawa, K. Takahashi, and M. Makimoto, "Miniaturized hairpin resonator filters and their application to receiver front-end MIC's," *IEEE Trans. Microwave Theory Tech.*, vol. 37, pp. 1991–1997, 1989.

[7] *EM User's Manual*, Sonnet Software, Inc., Version 2.4, 1993.

[8] J. D. Rhodes, "A low-pass prototype network for microwave linear phase filters," *IEEE Trans. Microwave Theory Tech.*, vol. MTT-18, pp. 290–301, 1970.

[9] J. S. Hong and M. J. Lancaster, "Couplings of microstrip square open-loop resonators for cross-coupled planar microwave filters," *IEEE Trans. Microwave Theory Tech.*, vol. 44, pp. 2099–2109, 1996.

[10] R. Levy, "Direct synthesis of cascaded quadruplet (CQ) filters," *IEEE Trans. Microwave Theory Tech.*, vol. 48, pp. 2940–2944, 1995.

[11] ———, "Filters with single transmission zeros at real or imaginary frequencies," *IEEE Trans. Microwave Theory Tech.*, vol. MTT-24, pp. 172–181, 1976.

Jia-Sheng Hong (M'94) received the D.Phil. degree in engineering science from Oxford University, Oxford, U.K., in 1994.

From 1979 to 1983, he worked at Fuzhou University, Fushou, as a Teaching/Research Assistant in radio engineering. In 1983, he was awarded a Friedrich Ebert Scholarship. He then visited Karlsruhe University, Germany, where he worked on microwave and millimeter-wave techniques from 1984 to 1985. In 1986, he returned to Fuzhou University as a Lecturer in microwave communications. In 1990, he was awarded a K. C. Wong Scholarship by Oxford University and became a graduate member of St. Peter's College at Oxford University, Oxford, U.K., where he conducted research in electromagnetic theory and applications. Since 1994, he has been a Research Fellow at Birmingham University, Birmingham, U.K. His current interests include RF and microwave devices for communications, microwave antennas, microwave applications of high-temperature superconductors, electromagnetic modeling, and the genetic approach for signal processing and optimization.

Michael J. Lancaster (M'91) received a degree in physics, in 1980, and the Ph.D. degree in 1984, for research into nonlinear underwater acoustics, both from Bath University, Bath, U.K.

After leaving Bath University, he joined the surface acoustic wave (SAW) group at the Department of Engineering Science at Oxford University, Oxford, U.K., as a Research Fellow. The research was in the design of new, novel SAW devices, including filters and filter banks. These devices worked in the frequency range 10 MHz–1 GHz. In 1987, he became a Lecturer at The University of Birmingham in the School of Electronic and Electrical Engineering, lecturing in electromagnetic theory and microwave engineering. Shortly after he joined the school, he began the study of the science and applications of high-temperature superconductors, working mainly at microwave frequencies. Currently, he heads the Electronic and Materials Devices group as a Reader. His present personal research interests include microwave filters and antennas, as well as the high-frequency properties and applications of a number of novel and diverse materials.

Dr. Lancaster is currently serving on the MTT-S International Microwave Symposium Technical Committee.